










Linear and spatial correlations of soil physical attributes in soybean cultivation under no-tillage system¹

Correlação linear e espacial dos atributos físicos do solo em soja sob sistema plantio direto

Nilton E. Mário^{*2}, Rafael Montanari², Lateiro S. de Sousa³, Neusa da E. Jorge Mário⁴,
Daniel C. Machado², Messias J. Eduardo², Juliana D. Pedroso²

¹ Research conducted at Universidade Estadual Paulista “Júlio de Mesquita Filho” (UNESP), Faculdade de Engenharia de Ilha Solteira (FEIS), Departamento de Fitossanidade, Engenharia Rural e Solos (DEFERS), Câmpus de Ilha Solteira, Ilha Solteira, São Paulo, Brasil

² Universidade Estadual Paulista “Júlio de Mesquita Filho”, Faculdade de Ciências Agrárias e Veterinárias (FCAV), Departamento de Ciência do Solo, Câmpus de Jaboticabal, SP, Brasil

³ Instituto Superior Politécnico de Gaza, Faculdade de Agricultura, Câmpus Politécnico de Lionde, Chókwè-Gaza, Moçambique

⁴ Faculdade de Tecnologia do Estado de São Paulo (FATEC), Câmpus Nilo De Stéfani, Jaboticabal, SP, Brasil

HIGHLIGHTS:

Surface layer shows higher variability and more attribute correlations, indicating increased management sensitivity.

Total soil DNA correlates with surface structure, confirming physical-biological integration under no-tillage.

Pure nugget effect suggests structural stability, restricting variable-rate management to texture and high spatial dependence.

ABSTRACT: This study aimed to evaluate the linear and spatial correlations of soil physical attributes in a soybean field under a no-tillage system in the 0.00–0.20 m and 0.20–0.40 m layers in Selvíria, Mato Grosso do Sul, Brazil. Soil sampling was carried out at 60 georeferenced points arranged in a 5 × 5 m experimental grid, considering soil texture (sand, clay, silt), porosity variables (Ma, Mi, dTP and cTP), density attributes (SD and PD), penetration resistance (PR_i and PR_b), gravimetric moisture (GM), and total soil deoxyribonucleic acid (DNAt). Data were analyzed using statistical and geostatistical techniques, with experimental semivariogram fitting and kriging interpolation. The surface layer showed greater variability and 23 significant linear correlations, including strong to very strong magnitudes between attributes, in contrast to the subsurface layer. DNAt was positively correlated with silt and negatively correlated with clay, indicating a physical-biological integration between soil structure and microbial activity. Most dynamic attributes exhibited a pure nugget effect, suggesting structural homogenization typical of consolidated and irrigated Oxisols under long-term no-tillage system, with variability restricted to the microscale. These results indicate that site-specific management should be targeted only to attributes with proven spatial dependence (silt, clay, and PR), whereas the remaining properties can be managed uniformly due to their intrinsic stability within the system.

Key words: soil layers, semivariograms, kriging maps, total soil DNA

RESUMO: O presente estudo objetivou avaliar a correlação linear e espacial de atributos físicos do solo em área sob cultivo de soja no sistema plantio direto nas camadas de 0,00–0,20 m e 0,20–0,40 m, em Selvíria-MS. A amostragem foi realizada em 60 pontos georreferenciados distribuídos em malha experimental de 5 × 5 m, considerando textura do solo (areia, argila, silte), variáveis de porosidade (Ma, Mi, PT_d e PT_c), atributos de densidade (DS e DP), resistência à penetração (RP_i e RP_b), umidade gravimétrica (UG) e ácido desoxirribonucleico total do solo (DNAt). A camada superficial apresentou maior variabilidade e 23 correlações lineares significativas, incluindo magnitudes fortes a muito fortes entre os atributos, em contraste com a subsuperficial. O DNAt correlacionou-se positivamente com o silte e negativamente com a argila, evidenciando integração físico-biológica entre estrutura e atividade microbiana. A maioria dos atributos dinâmicos exibiu efeito pepita puro, indicando homogeneização estrutural típica de Latossolos sob plantio direto consolidado e irrigado, com variabilidade restrita à microescala. Esses resultados indicam que o manejo em taxa variável deve ser aplicado apenas a atributos com dependência espacial comprovada (silte, argila e RP), enquanto os demais podem ser conduzidos de forma uniforme devido à estabilidade intrínseca do sistema.

Palavras-chave: camadas do solo, semivariogramas, mapas de krigagem, DNA total do solo



INTRODUCTION

Soybean plays a key role in the global agricultural sector due to its strong linkage with multiple industries. Rich in essential nutrients, it is widely used for food and feed production, primarily serving as a source of edible oil and protein for animal nutrition (Jiang et al., 2025).

Global soybean production is highly concentrated, with 80% originating from the United States, Brazil, and Argentina (Qiao et al., 2023). Within this context, Brazil has shown consistent growth in both cultivated area and grain yield in recent years. The 2024/25 growing season recorded an expansion to 47.35 million hectares (CONAB, 2025). In Mato Grosso do Sul state, the cultivated area reached 4.524 million hectares in the same season, with an average yield of 51.78 bags per hectare, resulting in a total production of 14.06 million tons (CONAB, 2025).

However, sustaining this production growth requires management practices that ensure long-term agricultural sustainability. Soil tillage plays a crucial role in shaping soil properties and ecosystem performance. The long-term effects of tillage on soil health are complex, site-specific, and dependent on crop type (Zapata et al., 2021). Conservation-oriented management practices can enhance multiple ecosystem services, helping to address emerging challenges associated with food security, poverty, and climate change impacts (Nurbekov et al., 2025).

Among the soil management systems used in soybean cultivation, the adoption of no-tillage (NT) has increased substantially. In Brazil, this system is widely consolidated across extensive agricultural areas, due to its documented long-term benefits for the soil in recent research (Torres et al., 2022). By minimizing soil disturbance, maintaining surface residue cover, and promoting soil aggregation via organic matter accumulation, NT enhances soil ecosystem services (Nurbekov et al., 2025). As a result, it improves soil physical and mechanical quality, offers protection against compaction, and increases macroporosity, favoring water infiltration and enhancing hydraulic conductivity (Bisolo et al., 2024).

Nevertheless, soil physical and chemical attributes exhibit high spatial variability, influenced by both natural factors and contrasting management practices (Silva et al., 2023). Such variability affects crop performance and may occur even within relatively small areas, in response to subtle differences in soil conditions (Martins et al., 2022).

Geostatistical techniques provide an effective alternative for analyzing the spatial behavior of soil attributes. Through the use of semivariograms, these techniques enable the identification of spatial range and dependence, providing essential parameters for mapping variability using kriging and/or cokriging methods (Dalchiavon & Carvalho, 2012).

However, most studies assessing the impact of soil management focus predominantly on shallow layers (0.10–0.15 m), despite the fact that root systems of most crops extend into deeper horizons (Thotakuri et al., 2024). Therefore, this study aimed to evaluate the linear and spatial correlations of soil physical attributes in a soybean field under a no-tillage system in the 0.00–0.20 m and 0.20–0.40 m layers in Selvíria, Mato Grosso do Sul, Brazil.

MATERIAL AND METHODS

The research was carried out in the municipality of Selvíria, MS, during the 2021/2022 agricultural season, spanning from November 2021 to May 2022. The geographic coordinates are 51° 22' West longitude of Greenwich and 20° 22' South latitude, with an altitude of 335 m. The location of the experimental area is presented below in Figure 1.

The soil was classified as Oxisol with a clayey texture (Soil Survey Staff, 2022). The climate classification of this region, according to Köppen's classification, is Aw, described as a humid tropical climate with a rainy season in the summer and a dry season in the winter (Alvares et al., 2014). The average annual temperature is 23.5 °C, the average annual rainfall is 1,370 mm, and the average annual relative humidity ranges between 70 and 80%. The location of the study area can be observed in Figures 1A and B.

The study area had been cultivated under a No-Tillage System (NTS) for more than ten years, adopting a crop rotation scheme alternating soybean and maize or sorghum during the summer, and pasture or black oat during the autumn–winter season, ensuring diverse soil cover and maintenance of soil organic matter. Part of the area was managed with soybean cultivation under a center pivot irrigation system, installed in 2013. Irrigation management was based on the crop water demand and local climatic conditions, with average irrigation depths ranging from 6 to 8 mm per application, applied at a frequency of two to three days, according to the soil water balance. Soil fertilization and correction were carried out according to the technical criteria of soil fertility established by Raij et al. (2001), based on chemical analysis of soil samples (0.00–0.20 m and 0.20–0.40 m). The last liming operation was performed in September 2015, with a surface application of 2.0 t ha⁻¹ of dolomitic limestone (Relative Neutralizing Value – RNV, 85%), without incorporation, complemented by phosphorus-based fertilization and the residual nutrient contribution from preceding cover crops. Weed control was carried out through pre-sowing desiccation with glyphosate herbicide (1,560 g ha⁻¹ of active ingredient), followed by mechanical shredding of crop residues using a horizontal shredder (Triton™), maintaining permanent soil mulch. Agricultural machinery traffic was minimized due to the no-tillage management, being limited to approximately three passes per growing cycle, corresponding to sowing, spraying, and harvesting operations, using medium-sized equipment.

Soil characterization was performed between late October and early November 2021, prior to the experiment installation. Subsequently, physical and chemical analyses were carried out at depths of 00.00–0.20 m and 0.20–0.40 m. Sampling locations were randomly selected within the soybean cultivation area. The soil had been managed under a NTS for approximately ten years and irrigated by a center pivot system. Research activities at the site began in 2013 under a history of annual crop rotation. The preceding crop was corn intercropped with Xaraés grass (*Urochloa brizantha* cv. Xaraés), and previous rotations included black oat, corn with Marandu grass, winter beans, and grass cultivated for straw production, aiming to maintain soil cover and promote system sustainability.

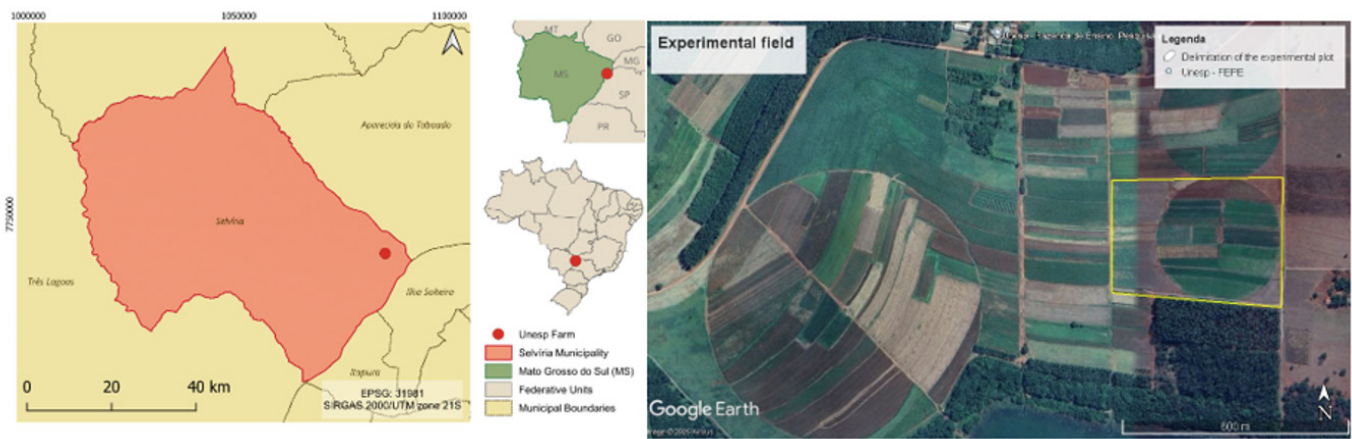


Figure 1. Location of the study area (A) and the experimental field with the sampling grid implementation (B)

To evaluate the spatial variability of soil physical attributes, a sampling grid was established within the irrigated NTS field. The spatial layout of the sampling grid was defined according to the Cartesian coordinate system (x and y axes), with a georeferenced starting point determined using an optical level. The grid was installed after soybean sowing, conducted in the first ten days of November 2021, covering an area of 15×70 m ($1,050$ m²). It consisted of four transects with fifteen sampling points each (4×15), totaling 60 regularly spaced sampling points at 5.00×5.00 m intervals, ensuring representative and homogeneous spatial distribution for the geostatistical analysis of soil physical attributes.

The studied soil physical attributes were individually determined and collected at layers of 0.00 - 0.20 m and 0.20 - 0.40 m, surrounding each sampling point.

The laboratory phase, which consisted of soil physical analyses, was carried out between March and May 2022. The determined soil attributes include: granulometry (sand, clay, and silt), macroporosity (Ma), microporosity (Mi), determined total porosity (dTP), soil density (SD), penetration resistance with impact penetrometer (PRi), penetration resistance with benchtop penetrometer (PRb), gravimetric moisture (GM), particle density (PD) and calculated total porosity (cTP). All soil physical attributes were determined following the methodology described by EMBRAPA (2018).

Total soil deoxyribonucleic acid (DNAt) was extracted following the method described by Plassart et al. (2012), with modifications in the cell disruption step, using a FastPrep homogenizer instead of manual agitation. Soil samples (0.25 g) were processed with glass beads and phosphate buffer, subjected to enzymatic lysis with lysozyme and proteinase K, followed by sodium dodecyl sulfate (SDS) treatment and freeze-thaw cycles to ensure complete cell rupture. DNA was precipitated with isopropanol, washed with 70% ethanol, resuspended in TE (Tris-EDTA) buffer, and stored at -20 °C until use. DNA quantification was performed according to Plassart et al. (2012) genomic system (GS) using a NanoDrop 2000c spectrophotometer, after system calibration and blank measurement with reference buffer to determine nucleic acid concentration and purity.

Also, for each attribute, spatial dependence was analyzed by calculating the semivariogram based on the assumptions

of stationarity and the intrinsic hypothesis. The spatialization of soil attributes was performed using block ordinary kriging (5.00×5.00 m) with the GS⁺ software.

Simple semivariograms were fitted for all studied attributes. The selection of the best-fit model followed a two-step procedure: initially, the highest coefficient of determination (R^2), the lowest sum of squared residual (SSR), and the highest degree of spatial dependence (DSD) were considered, as expressed in Eq. 1. The final decision regarding the most representative model, as well as the definition of the number of neighbors for interpolation, was based on cross-validation. From the fitted models, the nugget effect (C_0), sill ($C_0 + C_1$), and range (a) parameters were estimated. Additionally, cross-semivariograms were fitted among combinations of soil attributes as an exploratory analysis for potential co-kriging; however, the final interpolation used for map generation was based exclusively on univariate ordinary kriging.

$$DSD = \left[\frac{C}{(C + C_0)} \right] \times 100 \quad (1)$$

Where:

DSD - spatial dependence evaluator;

C_0 - structural variance; and,

$C + C_0$ - sill.

The proposed interpretation for the DSD was as established by Dalchiavon & Carvalho (2012): a) $DSD < 20\%$ = very low spatial dependence (VLD); b) $20\% \leq DSD < 40\%$ = low dependence (LD); c) $40\% \leq DSD < 60\%$ = moderate dependence (MD); d) $60\% \leq DSD < 80\%$ = high dependence (HD); and e) $80\% \leq DSD < 100\%$ = very high dependence (VHD).

Statistical analyses of the soil attributes were performed using SAS 9.4 software. Descriptive statistics, including mean, median, mode, minimum and maximum values, standard deviation, coefficient of variation, kurtosis, and skewness, were first calculated for each variable to characterize data distribution. Normality was assessed using the Shapiro-Wilk test. Subsequently, F-test was applied through the PROC GLM procedure to evaluate the statistical significance of differences in soil attributes between the two layers, considering significance of $p \leq 0.01$ and $p \leq 0.05$. The

variability of soil attributes was expressed by the coefficient of variation (CV), which was classified into four categories: low ($CV \leq 10\%$), medium ($10\% < CV \leq 20\%$), high ($20\% < CV \leq 30\%$), and very high ($CV > 30\%$), according to Keshavarzi et al. (2025). A simple linear correlation matrix was then generated using the PROC CORR procedure to determine Pearson's correlation coefficients (r) among soil attributes, providing a measure of the strength and direction of their linear relationships and revealing potential spatial associations within the dataset. Regression analyses were not performed because the objective was to identify associations among variables rather than establish predictive relationships.

RESULTS AND DISCUSSION

The results of descriptive statistics for the studied soil physical attributes in an irrigated area under a no-tillage planting system, at the sampling layers of 0.00 - 0.20 m and 0.20 - 0.40 m, are respectively presented in Table 1 and Table 2. In comparing the various soil attributes, both physical and chemical, the coefficient of variation directly influences the degree of variation in percentage terms. Thus, a higher percentage indicates greater data heterogeneity,

with the coefficient of variation (CV) serving as a tool for analyzing this variability.

When analyzing the data presented in Tables 1 and 2, it was observed that the soil attributes in the 0–20 cm and 20–40 cm layers reveal a highly compartmentalized ecosystem. The intrinsic properties of the mineral matrix, such as PD, CLA, and SAN, exhibited low variability ($CV < 10\%$), establishing a stable structural foundation upon which the system's functional heterogeneity emerges. In the surface layer (0–20 cm), biological heterogeneity remains a key component of the system's dynamics, as indicated by a mean total soil DNA (DNAt) concentration of $243.2 \text{ ng } \mu\text{L}^{-1}$ and a coefficient of variation of 15.3 %. This variability is consistent with the occurrence of microbial "hotspots" promoted by the absence of tillage and the accumulation of crop residues in consolidated NTS, which can generate sharp micro-scale gradients in moisture, residue decomposition, and localized compaction (Neupane et al., 2022). However, part of the spatial signal captured by DNAt may arise not only from true biological activity but also from the uneven distribution of relic DNA, the extracellular, persistent fraction of DNAt that becomes adsorbed to Fe and Al oxides and mineral surfaces (Freeman et al., 2023). Such adsorption enhances the stability of genetic material in the soil,

Table 1. Descriptive statistics of soil physical attributes of an Oxisol at 0–0.20 m layer under no-tillage in an irrigated area

Attribute ^(a)	Descriptive statistical measures									
	Mean	Median	Value		Standard deviation	Coefficient			Test probability ^(b)	
			Minimum	Maximum		Variation (%)	Kurtosis	Skewness	Pr<w	FD
PR ₁ (MPa)	1.85	1.85	1.12	2.91	0.34	18.41	1.90	0.91	0.005	IN
GM ₁ (kg kg ⁻¹)	0.25	0.23	0.05	0.67	0.08	33.02	12.72	2.49	0.000	IN
PD ₁ (kg dm ⁻³)	2.52	2.50	2.44	2.60	0.03	1.10	1.90	0.77	0.000	IN
CLA ₁ (g kg ⁻¹)	491.6	487.5	427	594	33.07	6.73	0.56	0.59	0.194	NO
SAN ₁ (g kg ⁻¹)	410.12	412.00	297.00	473.00	34.78	8.48	1.78	-0.79	0.017	IN
SIL ₁ (g kg ⁻¹)	97.38	96.00	38.00	157.00	24.83	25.50	-0.11	0.06	0.952	NO
Ma ₁ (m ³ m ⁻³)	0.07	0.06	0.01	0.15	0.03	36.40	1.69	1.11	0.000	IN
Mi ₁ (m ³ m ⁻³)	0.22	0.22	0.10	0.38	0.04	18.71	8.18	1.46	0.000	IN
SD ₁ (kg dm ⁻³)	1.50	1.52	1.13	1.76	0.13	8.55	0.25	-0.61	0.059	NO
dTP ₁ (m ³ m ⁻³)	0.28	0.27	0.17	0.45	0.04	14.55	4.76	1.33	0.000	IN
PRb ₁ (MPa)	1.67	1.64	0.62	2.85	0.47	28.17	-0.09	0.14	0.992	NO
cTP ₁ (m ³ m ⁻³)	0.40	0.40	0.30	0.55	0.05	12.65	0.10	0.53	0.187	NO
DNAt (ng/μl)	243.20	245.50	152.00	329.00	37.10	15.30	-0.20	0.11	0.759	NO

^(a)PR, GM, PD, CLA, SAN, SIL, Ma, Mi, SD, dTP, PRb, cTP, and DNAt are, respectively, penetration resistance, gravimetric moisture, particle density, clay, sand, silt, macroporosity, microporosity, soil density, determined total porosity, penetration resistance by benchtop analysis, calculated total porosity, and total soil deoxyribonucleic acid; ^(b)FD - Frequency distribution, where NO and IN represent normal and indeterminate types, respectively

Table 2. Descriptive statistics of soil physical attributes of an Oxisol at 0.20–0.40 m layer under no-tillage in an irrigated area

Attribute ^(a)	Descriptive statistical measures									
	Mean	Median	Value		Standard deviation	Coefficient			Test probability ^(b)	
			Minimum	Maximum		Variation (%)	Kurtosis	Skewness	Pr<w	FD
PR ₂ (MPa)	2.08	2.01	1.19	3.25	0.38	18.50	1.92	0.97	0.00	IN
GM ₂ (kg kg ⁻¹)	0.29	0.24	0.02	0.61	0.22	78.21	25.08	4.78	0.00	IN
PD ₂ (kg dm ⁻³)	2.57	2.57	2.50	2.67	0.05	1.74	-0.52	0.19	0.00	IN
CLA ₂ (g kg ⁻¹)	520.53	520.00	428.00	591.00	31.12	5.98	0.53	-0.33	0.85	NO
SAN ₂ (g kg ⁻¹)	389.38	392.00	299.00	468.00	34.10	8.76	-0.10	-0.12	0.68	NO
SIL ₂ (g kg ⁻¹)	90.22	88.00	62.00	164.00	20.65	22.89	1.72	1.08	0.00	IN
Ma ₂ (m ³ m ⁻³)	0.09	0.07	0.04	0.51	0.08	86.56	19.30	4.28	0.00	IN
SD ₂ (kg dm ⁻³)	1.49	1.49	1.19	1.76	0.11	7.56	0.72	-0.54	0.12	NO
dTP ₂ (m ³ m ⁻³)	0.30	0.29	0.17	0.71	0.07	22.88	25.14	4.27	0.00	IN
Mi ₂ (m ³ m ⁻³)	0.20	0.22	0.02	0.27	0.04	20.45	9.88	-2.93	0.00	IN
PRb ₂ (kPa)	1.59	1.58	0.86	2.39	0.37	23.40	-0.61	0.16	0.52	NO
cTP ₂ (m ³ m ⁻³)	0.42	0.42	0.31	0.53	0.05	10.94	0.10	0.25	0.29	NO

^(a) PR, GM, PD, CLA, SAN, SIL, Ma, Mi, SD, dTP, PRb, and cTP, are, respectively, penetration resistance, gravimetric moisture, particle density, clay, sand, silt, macroporosity, microporosity, soil density, determined total porosity, penetration resistance by benchtop analysis, and calculated total porosity; ^(b) FD - Frequency distribution, where NO and IN represent normal and indeterminate types, respectively

prolonging its persistence and potentially inflating estimates of microbial biomass. Therefore, the observed CV likely reflects the combined effects of biological heterogeneity and physicochemical accumulation of relic DNA, confirming DNA_t as a sensitive—yet spatially structured—indicator of soil biogeochemical dynamics in mature NTS.

The high variability of Ma₁ (CV = 36.4%) and GM₁ (CV = 33.0%) reflects the direct influence of biological processes on soil physical structure. In the subsurface (20–40 cm), structural and hydraulic heterogeneity becomes more pronounced, with extreme values for Ma₂ (CV = 86.6%) and GM₂ (CV = 78.2%), revealing the close relationship between irregular macropore networks and preferential water flow. PR₂ showed only moderate variability (CV = 18.5%), suggesting that the system's complexity is more related to pore architecture than to the density of the solid matrix. This integrated configuration, of a biologically heterogeneous surface driving an increasingly variable structural and hydraulic subsurface, explains the divergence observed relative to Mário et al. (2024), likely resulting from differences in soil type and the duration of NT adoption, since less clayey soils or recently established systems tend to exhibit lower structural maturity (Chakraborty et al., 2022).

The analysis of soil attribute variability presented in Tables 1 and 2 revealed a complex signature resulting from the interplay between soil type and management history. Attributes associated with pore structure and mechanical resistance, such as Mi₂, dTP₂, and PRb_{1,2}, exhibited high variability (CV ranging from 20.5 to 28.2%). This behavior

is characteristic of consolidated NTS, in which machinery traffic and biological activity promote a heterogeneous spatial redistribution of soil structure (Chakraborty et al., 2022). In contrast, our results differ from those reported by Silva et al. (2023), who observed very high variability in penetration resistance in highly clayey Oxisols, likely due to their greater susceptibility to compaction under heavier machinery loads. Such divergence probably reflects differences in management intensity and soil texture, since more clayey soils under intense traffic tend to develop stronger density contrasts. Even more revealing is the unusually high variability in the silt fraction (SIL_{1,2}), with CVs between 22.9 and 25.5%, a pattern atypical of Oxisols that generally display low textural dispersion due to their pedogenic stability (Laurenti et al., 2024). This anomaly suggests a particular pedogenetic history for the study area, possibly related to erosional and depositional processes introducing textural heterogeneity (Totti et al., 2025). Therefore, the observed discrepancies do not represent contradictions but rather complementary evidence that the current soil structure reflects both recent no-tillage management, especially the duration and intensity of machinery traffic, and its pedogenetic legacy.

The normal frequency distribution, which is typical of soil data, is considered ideal for both statistical and geostatistical analyses, as it ensures consistency and representativeness in spatial interpolation models (Álvarez-Herrera et al., 2025). However, when data does not follow a normal distribution, researchers often apply logarithmic or Box-Cox transformations to improve model accuracy and predictive

performance (Keshavarzi et al., 2025). The soil physical attributes that exhibited negative skewness coefficients were SAN₁, dTP₁, CLA₂, SAN₂, SD₂, and Mi₂. Similarly, negative kurtosis coefficients were found for SIL₁, PRb₁, DNAt, PD₂, SAN₂, and PRb₂. The remaining attributes displayed positive kurtosis values, corresponding to normal (N) frequency distributions, except for SAN₁, dTP₁, Mi₂, and PD₂, which exhibited indeterminate (IN) distributions. For CLA_{1,2}, SAN₂, SIL₁, SD_{1,2}, PRb_{1,2}, cTP_{1,2}, and DNAt, the frequency distribution was normal (N), while for the other attributes, it was indeterminate (IN). Data anomalies may be related to sampling errors or soil heterogeneity caused by recent mechanization impacts. These patterns differ from those observed by Nidhi et al. (2025), who reported non-normal distributions for similar soil attributes in alluvial Oxisols under varying management conditions. The coexistence of indeterminate (IN) and normal (N) distributions is not merely a statistical feature but reflects soil heterogeneity and complex interactions with management factors, particularly the influence of mechanization, which can induce non-random spatial variations. Overall, the skewness coefficients were close to zero, indicating approximately symmetric distributions (Keshavarzi et al., 2025).

According to Tables 3 and 4, the correlation matrices show the simple linear correlations between soil physical attributes versus soil physical attributes at the depth of 0.00 - 0.20 m (PRi₁, GM₁, PD₁, CLA₁, SAN₁, SIL₁, Ma₁, Mi₁, SD₁, dTP₁, PRb₁, cTP₁, and DNAt) and at the depth of 0.20 - 0.40 m (PRi₂, GM₂, PD₂, CLA₂, SAN₂, SIL₂, Ma₂, Mi₂, SD₂, dTP₂, PRb₂, and cTP₂) under irrigated no-tillage. Significant correlations can be observed in the first layer (0.00-0.20 m) (Table 3) for the following pairs: SIL₁ × PRi₁, CLA₁ × GM₁, SAN₁ × GM₁, SIL₁ × PD₁, SAN₁ × CLA₁, SIL₁ × CLA₁, SIL₁ × SAN₁, Mi₁ × SAN₁, SD₁ × Mi₁, dTP₁ × Ma₁, dTP₁ × Mi₁, dTP₁ × SD₁, PRb₁ × Ma₁, PRb₁ × SD₁, PRb₁ × dTP₁, cTP₁ × Ma₁, cTP₁ × Mi₁, cTP₁ × SD₁, cTP₁ × dTP₁, cTP₁ × PRb₁,

DNAt × CLA₁, DNAt × SIL₁ and DNAt × PRb₁, and in the second layer (0.20-0.40 m) (Table 4) for the following pairs: CLA₂ × PRi₂, SAN₂ × PRi₂, Mi₂ × PRi₂, SAN₂ × PD₂, SAN₂ × CLA₂, Mi₂ × CLA₂, dTP₂ × CLA₂, SIL₂ × SAN₂, Mi₂ × SAN₂, Mi₂ × Ma₂, dTP₂ × Ma₂, SD₂ × Mi₂, cTP₂ × Mi₂, PRb₂ × SD₂, cTP₂ × SD₂ and cTP₂ × PRb₂.

All pairs that showed positive correlations in the 0.00–0.20 m and 0.20–0.40 m layers are directly proportional, indicating that an increase in one attribute leads to a simultaneous increase in the other. Conversely, the pairs that displayed negative correlations reveal inverse relationships, where an increase in one variable corresponds to a decrease in the other.

The negative correlation between cTP and PRb in both layers shows that higher total porosity leads to lower penetration resistance. This occurs because the Latosol structure acts as a stress-dissipating network in which greater pore connectivity promotes elastic deformation and reduces internal friction. As a result, applied loads are distributed more evenly, lowering mechanical impedance and improving root penetration. Chakraborty et al. (2022) found similar behavior in managed Oxisols, where enhanced microporosity and pore connectivity reduced compaction and improved soil physical quality.

The pairs dTP₁ × Mi₁, Mi₂ × Ma₂, and dTP₂ × Ma₂ demonstrate the balance between pore fractions that simultaneously controls aeration and water retention. Increases in macroporosity improve infiltration and oxygen diffusion, while reducing water storage in micropores. Bisolo et al. (2024) reported that conservation systems such as no-tillage and crop-livestock integration preserve this balance through root activity and surface residue protection. These findings highlight the importance of maintaining soil cover and managing machinery traffic to sustain porosity and hydrological efficiency.

The inverse correlation between dTP₁ and SD₁ represents a physical expression of compaction: as the pore volume

Table 3. Correlation matrix of soil attributes in an Oxisol at 0.00–0.20 m depth under no-tillage in an irrigated area

Attributes ^(a)	PRi ₁	GM ₁	PD ₁	CLA ₁	SAN ₁	SIL ₁	Ma ₁	Mi ₁	SD ₁	dTP ₁	PRb ₁	cTP ₁	DNAt
PRi ₁	-												
GM ₁	0.16	-											
PD ₁	-0.09	-0.06	-										
CLA ₁	-0.13	0.34**	-0.01	-									
SAN ₁	-0.06	-0.29*	-0.18	-0.72**	-								
SIL ₁	0.28*	-0.04	0.29*	-0.28*	-0.44**	-							
Ma ₁	-0.17	-0.02	-0.03	0.01	0.07	-0.15	-						
Mi ₁	0.02	0.09	-0.01	0.03	-0.25*	0.18	0.00	-					
SD ₁	0.12	-0.09	0.08	0.02	0.08	-0.14	-0.28	-0.35**	-				
dTP ₁	0.00	0.11	-0.01	0.14	-0.19	0.09	0.56**	0.65**	-0.52**	-			
PRb ₁	-0.04	-0.02	0.10	-0.04	-0.04	0.09	-0.52**	-0.15	0.33**	-0.53**	-		
cTP ₁	-0.14	0.08	0.05	-0.03	-0.10	0.17	0.28*	0.34**	-0.99**	0.52**	-0.32*	-	
DNAt	0.12	-0.14	0.06	-0.27*	0.01	0.30*	-0.19	0.02	0.14	-0.18	0.31*	-0.13	-

^(a) PR, GM, PD, CLA, SAN, SIL, Ma, Mi, SD, dTP, PRb, cTP, and DNAt are, respectively, penetration resistance, gravimetric moisture, particle density, clay, sand, silt, macroporosity, microporosity, soil density, determined total porosity, penetration resistance by benchtop analysis, calculated total porosity; ^(b) * Significant at p ≤ 0.05, ** Significant at p ≤ 0.01

Table 4. Correlation matrix of soil attributes in an Oxisol at 0.20–0.40 m depth under no-tillage in an irrigated area

Attributes ^(a)	PR ₂	GM ₂	PD ₂	CLA ₂	SAN ₂	SIL ₂	Ma ₂	Mi ₂	SD ₂	dTP ₂	PRb ₂	cTP ₂
PR ₂	-											
GM ₂	-0.02	-										
PD ₂	0.15	-0.04	-									
CLA ₂	0.33*	0.11	0.23	-								
SAN ₂	-0.29*	-0.04	-0.27*	-0.80**	-							
SIL ₂	0.06	-0.09	0.07	0.00	-0.54**	-						
Ma ₂	-0.09	-0.00	0.10	0.11	-0.05	-0.07	-					
Mi ₂	0.41**	-0.06	0.03	0.26*	-0.27*	0.03	-0.50**	-				
SD ₂	-0.20	0.12	-0.07	-0.81	0.02	0.06	-0.00	-0.26*	-			
dTP ₂	0.14	-0.04	0.20	0.29*	-0.22	-0.07	0.85**	0.01	-0.17	-		
PRb ₂	-0.01	0.01	0.06	-0.04	0.04	-0.07	0.01	-0.15	0.53**	-0.07	-	
cTP ₂	0.23	-0.10	0.17	0.14	-0.11	-0.01	0.03	0.32*	-0.95**	0.20	-0.51**	-

^(a) PR, GM, PD, CLA, SAN, SIL, Ma, Mi, SD, dTP, PRb, and cTP, are, respectively, penetration resistance, gravimetric moisture, particle density, clay, sand, silt, macroporosity, microporosity, soil density, determined total porosity, penetration resistance by benchtop analysis, and calculated total porosity; ^(b) * Significant at $p \leq 0.05$, ** Significant at $p \leq 0.01$

decreases, bulk density rises, and the soil matrix becomes more rigid. Moraes et al. (2024) quantified this relationship by modeling penetration resistance as an exponential function of bulk density and soil moisture, demonstrating that structural compression reduces both elasticity and rehydration capacity. Under continuous mechanical stress, clay bridges and organic colloids rearrange, creating a denser, less resilient structure. For sustainable management, field operations should be restricted to near-optimal moisture conditions, avoiding the plastic deformation that occurs when soils are saturated and more susceptible to irreversible compaction.

Negative correlations among SIL \times SAN, CLA \times SAN, and Mi \times SAN confirm the strong influence of texture on the soil's physical–hydraulic regime. As sand content increases, the number of water-retaining micropores declines, reducing the soil's capacity to hold plant-available water and increasing susceptibility to surface sealing. Totti et al. (2025) observed that higher clay contents enhance structural stability, aggregate cohesion, and carbon retention in Oxisols and Ultisols, leading to improved resistance against compaction. In the present study, the predominance of clay in the Oxisol contributed to higher microporosity and better water storage, though possibly at the expense of aeration under near-saturated conditions. This highlights the need for management strategies that balance aeration and retention, particularly in regions with alternating wet and dry periods.

The positive correlation between PR and SD demonstrates that denser soils exhibit greater mechanical impedance. This occurs because compaction reduces the interaggregate voids that normally facilitate gas and water exchange, thereby increasing rigidity. Álvarez-Herrera et al. (2025) found that such densification restricts water redistribution and gas diffusion, creating physical barriers to root elongation. In practice, continuous organic residue input, maintenance of surface cover, and reduced traffic intensity are effective in mitigating this structural stiffening, ensuring that the soil retains adequate porosity and mechanical resilience.

Correlations involving SIL \times PD, SIL \times CLA, and SAN \times PD showed distinct patterns compared with findings from Totti et al. (2025) in other Red Latosols, indicating that the mineralogical composition exerts a dominant influence on particle density and aggregate stability. The higher contents of Fe and Al oxides in this soil enhance cementation and interaggregate cohesion, leading to greater structural persistence but also to higher particle density. This mechanism reflects the typical microstructure of highly weathered Latosols, where oxides bind clay domains into stable microaggregates, reducing the dispersion potential. Consequently, these soils respond differently to compaction stress than less weathered or quartz-dominated systems, maintaining cohesion even under intensive management. Such characteristics must be considered in mechanization and traffic control, as excessive stress can exceed the soil's elastic recovery capacity, compromising macroporosity and root penetration.

In contrast, the positive correlations found for dTP \times CLA and Mi \times CLA agree with results by Chakraborty et al. (2022), who also observed that higher clay contents enhance total porosity and microporosity in Red-Yellow Latosols under managed systems. The predominance of clay minerals and Fe/Al oxides promotes strong aggregation and internal pore continuity, improving water retention and hydraulic conductivity. The inverse relationships involving SIL \times CLA and SAN \times PD reinforce the textural control over density and structural arrangement, showing that fine-textured fractions contribute to a more cohesive and porous matrix. Therefore, the clay fraction acts as the structural core regulating both physical resilience and hydraulic functionality. Maintaining this equilibrium through conservation tillage, residue retention, and diversified rooting systems is critical for sustaining soil structure, water dynamics, and long-term productivity in tropical NT environments.

Table 5 shows the parameters of the fitted semivariograms for some physical attributes of a dystrophic Red Latosol under

irrigated no-tillage at depths of 0.00-0.20 m and 0.20-0.40 m under soybean cultivation. It was found that, except for PRi_2 , CLA_1 , SIL_1 , Ma_1 , PRb_2 , and DNA_1 , which showed spatial dependence, all other attributes exhibited a pure nugget effect.

The occurrence of a pure nugget effect indicates that these attributes are spatially independent, have a random distribution, or that the sampling grid spacing is larger than necessary to reveal spatial dependence (Keshavarzi et al., 2025).

Regarding the performance of the semivariograms, a decreasing relationship was established based on the analysis of the magnitude of the spatial coefficient of determination (r^2), as follows: 1) SIL_1 , 2) CLA_1 , 3) PRb_2 , 4) DNA_1 , 5) PRi_2 , and 6) Ma_1 . However, concerning the first three attributes (SIL_1 , CLA_1 , and PRb_2), which showed a high spatial coefficient of determination, the following was observed, as reported below:

For the first attribute (SIL_1), the R^2 value (0.968) indicated the most robust semivariogram fit, consistent with Filintas (2025) and in line with the findings of Martins et al. (2022), who reported strong spatial dependence for textural fractions in Oxisols under conservation management, but differing from Souza et al. (2023), who observed a pure nugget effect for silt and clay in sugarcane fields. The exponential model and a DSD of 88% demonstrated a highly structured spatial pattern, with a range of 53.4 m, and the sampling grid of sixty georeferenced points spaced at 5×5 m across a 15×70 m area provided sufficient resolution to detect large-scale spatial dependence. The occurrence of pure nugget effects in almost half of the attributes does not indicate insufficient sampling density but rather reflects a soil matrix whose physical organization has reached a high degree of uniformity under long-term no-tillage and continuous irrigation. This interpretation is reinforced by

Table 5. Parameters of the fitted simple semivariograms for soil attributes in an Oxisol under no-tillage in an irrigated area at layers of 0.00–0.20 m and 0.20–0.40 m

Attributes ^(a)	Parameters							Degree of spatial dependence	
	Model ^(b)	Nugget effect (C_0)	Sill ($C_0 + C$)	Range (A_0) (m)	R^2	SSR ^(c)	DSD ^(d)	Class ^(e)	
PRi_1	pne	-	0.107	-	-	-	-	-	
PRi_2	exp	0.012	0.105	27.60	0.805	$1.759 \cdot 10^{-4}$	88%	VHD	
GM_1	pne	-	0.0064	-	-	-	-	-	
GM_2	pne	-	0.0055	-	-	-	-	-	
PD_1	pne	-	0.00066	-	-	-	-	-	
PD_2	pne	-	0.00193	-	-	-	-	-	
CLA_1	exp	47.00	1078.0	39.90	0.94	11493	95%	VHD	
CLA_2	pne	-	2369.0	-	-	-	-	-	
SAN_1	pne	-	2834.0	-	-	-	-	-	
SAN_2	pne	-	2760.0	-	-	-	-	-	
SIL_1	exp	75.0	654.80	53.40	0.968	2790	88%	VHD	
SIL_2	pne	-	426.30	-	-	-	-	-	
Ma_1	sph	0.00013	0.0008	28.40	0.721	$3.71 \cdot 10^{-8}$	83%	VHD	
Ma_2	pne	-	0.0065	-	-	-	-	-	
Mi_1	pne	-	0.0019	-	-	-	-	-	
Mi_2	pne	-	0.0016	-	-	-	-	-	
SD_1	pne	-	0.0165	-	-	-	-	-	
SD_2	pne	-	0.012	-	-	-	-	-	
dTP_1	pne	-	0.0018	-	-	-	-	-	
dTP_2	pne	-	0.0052	-	-	-	-	-	
PRb_1	pne	-	0.228	-	-	-	-	-	
PRb_2	gau	0.0229	0.1478	15.76	0.890	$1.41 \cdot 10^{-4}$	84%	VHD	
cTP_1	pne	-	0.0026	-	-	-	-	-	
cTP_2	pne	-	0.0024	-	-	-	-	-	
DNA_1	sph	593.0	1372.0	30.0	0.826	29260	56%	MD	

^(a) PRi , GM , PD , CLA , SAN , SIL , Ma , Mi , SD , dTP , PRb , cTP , and DNA_1 are, respectively, penetration resistance, gravimetric moisture content, particle density, clay, sand, silt, macroporosity, microporosity, soil density, determined total porosity, penetration resistance by benchtop analysis, calculated total porosity, and total soil deoxyribonucleic acid. ^(b)gau - Gaussian; exp - Exponential; sph - Spherical; pne - Pure nugget effect; ^(c)SSR - Sum of squared residuals; ^(d)DSD - Evaluator of the degree of spatial dependence; ^(e)VHD - Very high dependence, MD - Moderate dependence

Torres et al. (2022), who associated no-tillage and irrigation with the homogenization of physical and hydraulic properties in the surface layer. The microaggregate structure and stable porosity typical of Oxisols minimize spatial contrasts, causing variations in dynamic attributes to occur at scales smaller than the sampling interval. Therefore, the absence of spatial dependence in several attributes arises more from structural resilience and management-induced homogenization than from random variability. In this context, silt stands out as one of the few fractions still capable of expressing a measurable spatial gradient due to its mineralogical persistence and resistance to management disturbances. This structural regularity, supported by the recommendation of Breure et al. (2022) to focus site-specific management on attributes with verified spatial dependence, suggests that system uniformity should be interpreted as advantageous, as it reflects high structural stability and lower susceptibility to degradation.

For the second attribute (CLA_1), the R^2 value (0.940) confirmed a strong spatial fit, supported by a DSD of 95% and an exponential model with a 39.9 m range, consistent with Martins et al. (2022), who observed persistent spatial dependence of clay in conservation-managed Oxisols, and corroborated by Torres et al. (2022), who associated irrigation with structural homogenization in surface layers. In contrast, Souza et al. (2023) reported predominantly random distributions and pure nugget effects for fine fractions in sugarcane soils, highlighting that management history plays a decisive role in shaping spatial behavior. Clay's strong spatial structure thus contrasts with the lack of dependence observed in many other variables, reinforcing its role as a key determinant of physical organization. The dense 5×5 m sampling grid rules out any hypothesis of inadequate resolution; rather, the predominance of pure nugget effects in other attributes reflects the cumulative influence of irrigation, organic inputs, and reduced mechanical disturbance, conditions known, as emphasized by Filintas (2025), to promote microaggregate stability and attenuate spatial contrasts. In such systems, the redistribution of fine particles and consolidation of microaggregates create a homogeneous microstructure that suppresses spatial variability beyond the microscale. This explains why clay retains spatial coherence while dependent properties, such as porosity and bulk density, display random or undetectable patterns. The observed uniformity reflects equilibrium, not randomness: a stable arrangement of fine particles that ensures high physical resilience. From a management perspective, this equilibrium supports the proposition of Breure et al. (2022) that site-specific interventions should target only attributes with proven spatial dependence. Even in uniform systems, the strong linkage between clay, microporosity, and total porosity highlights that clay-enriched zones remain fundamental to maintaining water retention and structural stability, reinforcing the importance of organic matter maintenance and controlled machinery traffic.

For the third attribute (PRb_2), the r^2 value (0.890) indicated the third-best semivariogram fit, contrasting with the findings of Rodrigues et al. (2023), who, while examining the spatial correlation of soybean yield with the chemical attributes of an Oxisol, reported a pure nugget effect for penetration

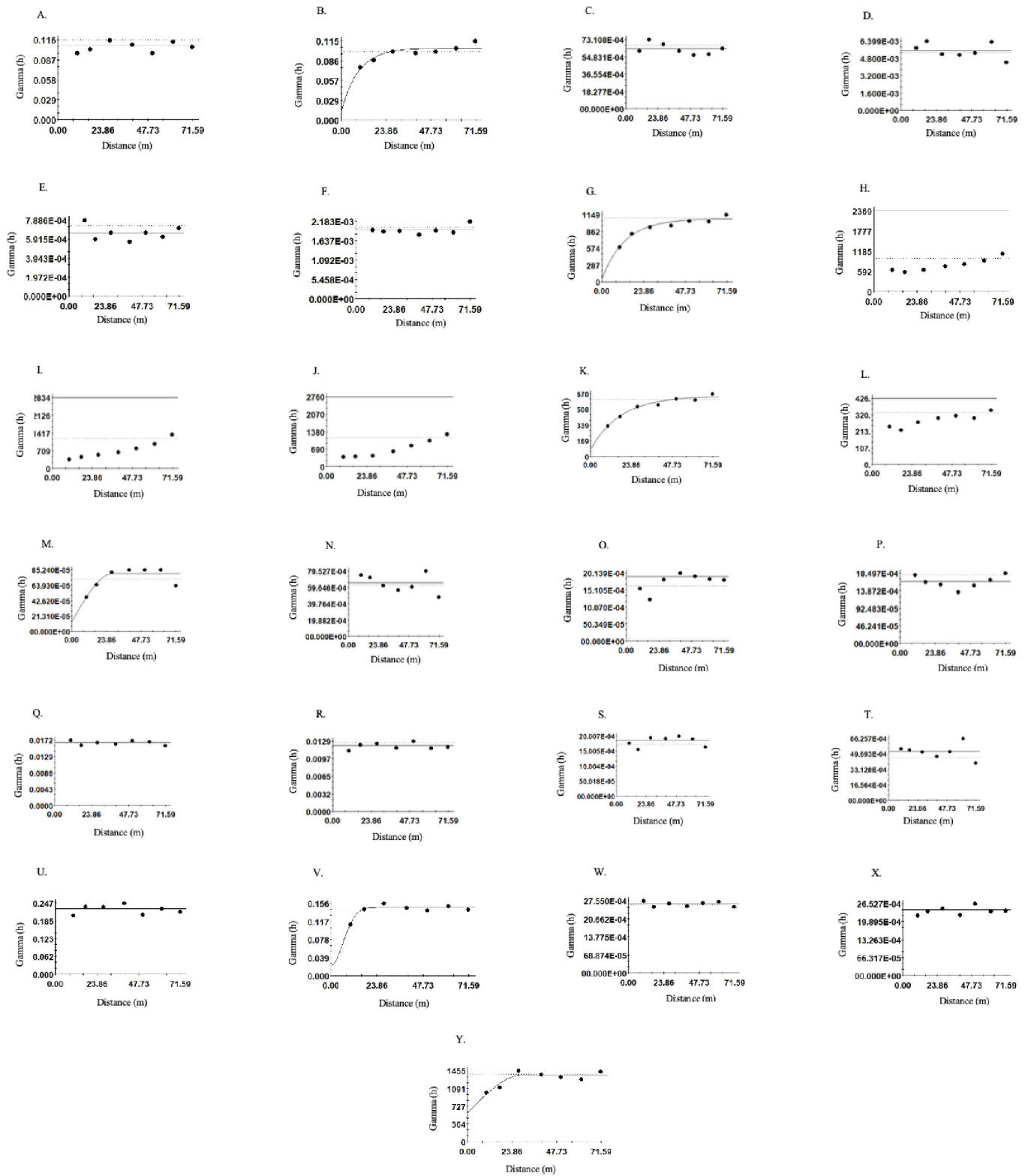
resistance. With a DSD of 84%, PRb_2 exhibits very high spatial dependence, indicating that its variability follows a structured spatial pattern. This information enables the implementation of site-specific management strategies, such as targeted soil compaction adjustments and localized input applications, aiming to optimize productivity and mitigate negative impacts of machinery traffic. Understanding the spatial behavior of PRb_2 allows for targeted interventions, emphasizing the importance of planning agricultural operations based on attributes with proven spatial dependence to maximize system efficiency and sustainability.

The semivariogram range analysis presented in Table 5 showed the following decreasing sequence: SIL_1 (53.40 m), CLA_1 (39.90 m), $DNAt$ (30.0 m), Ma_1 (28.40 m), PRi_2 (27.60 m), and PRb_2 (15.76 m). These values represent the spatial extent over which attribute variability can be considered correlated. For future studies and precision agriculture applications, ranges should not be set below 15.76 m, corresponding to the smallest observed value, to ensure that spatial models adequately capture soil variability. From a management perspective, this information has direct practical implications: site-specific interventions, such as soil correction, fertilizer application, or machinery traffic adjustments, should be planned considering minimum areas close to the determined ranges, thereby optimizing operational efficiency while respecting the true spatial variability of soil attributes.

Simple-semivariograms between soil attributes in an Oxisol under a no-tillage system are presented in Figures 2A–Y.

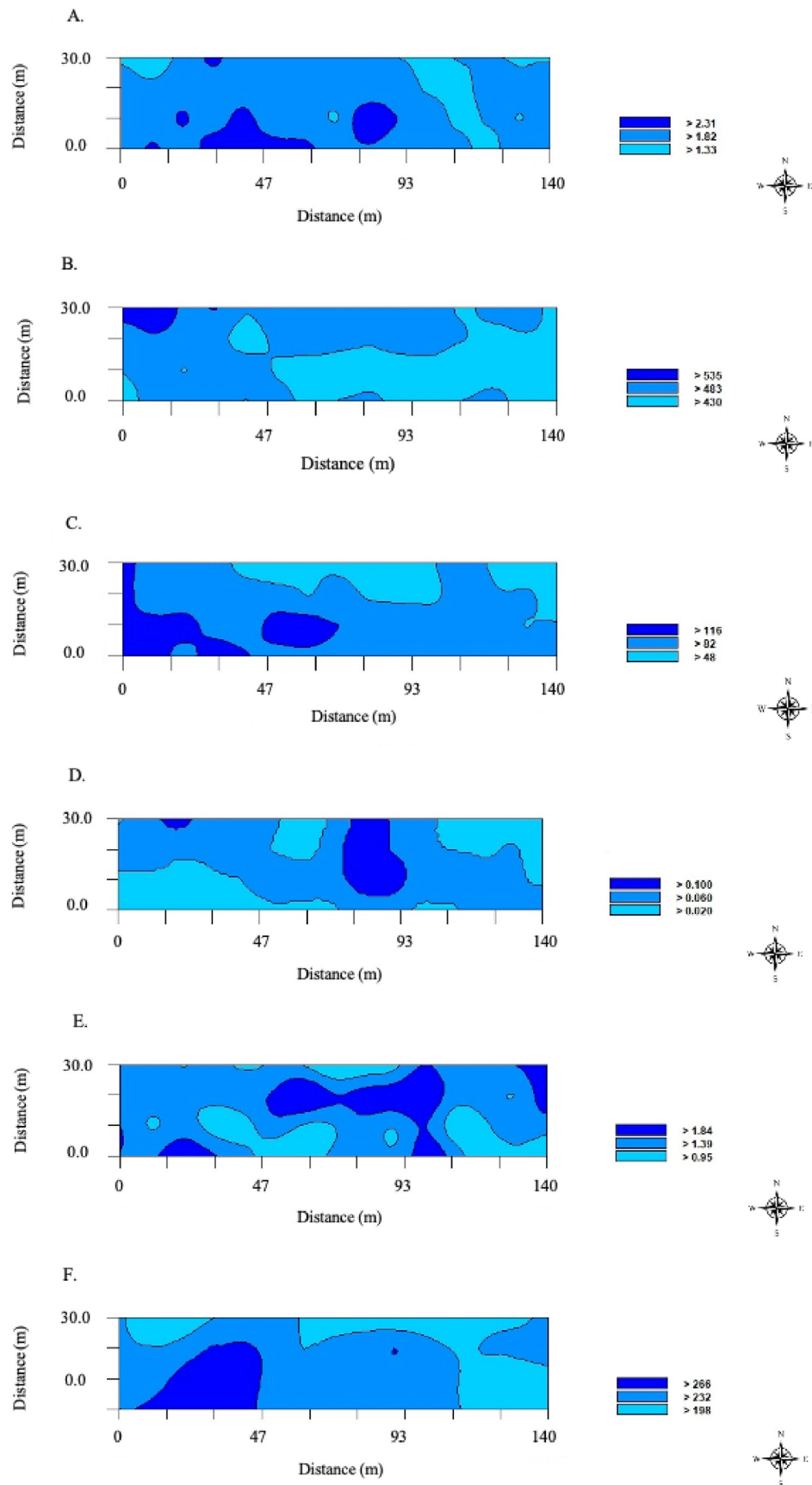
In Figures 3A–F, kriging maps are presented showing the soil attributes of an Oxisol in the municipality of Selvíria - MS, for soybean cultivation under a no-tillage system. Among the maps displayed below, we will comment on those that show high spatial similarity for practical soil management purposes. Accordingly, the following physical attributes were found to exhibit such similarity: PRi_2 , CLA_1 , SIL_1 , Ma_1 , PRb_2 , and $DNAt$.

In Figure 3A, it is evident that the southwestern portion of the study area exhibits higher levels of soil penetration resistance (PRi_2), reaching 2.31 MPa in the second layer. Rodrigues et al. (2023) reported a negative relationship between soil compaction and soybean grain yield, observing lower yields and increased resistance values, with negative correlations of 40 and 33% in the 2017 and 2018 growing seasons, respectively. For producers, such compaction in the southwestern area implies a physical limitation to root growth and consequently reduced yield potential. Therefore, these zones should be prioritized for soil decompaction strategies, either mechanical or biological, through the adoption of deep-rooted cover crops and controlled-traffic farming systems to minimize additional structural degradation. Furthermore, in the northwestern region, although it represents a relatively small portion of the map, soils with higher clay content in the first layer (CLA_1) were identified, reaching 535 g kg^{-1} , while lower clay values were observed in the southern, southeastern, and eastern areas. These findings corroborate those of Souza et al. (2023), who also reported elevated clay fractions in the surface horizon. From a management perspective, areas with higher clay content require careful irrigation scheduling and nutrient management due to their greater water-holding capacity, which may promote anaerobic conditions under excessive moisture. Conversely, the



PR₁ and PR₂ – penetration resistance, GM₁ and GM₂ - gravimetric moisture, PD₁ and PD₂ - particle density, CLA₁ and CLA₂ - clay, SAN₁ and SAN₂ - sand, SIL₁ and SIL₂ - silt, Ma₁ and Ma₂ - macroporosity, Mi₁ and Mi₂ - microporosity, SD₁ and SD₂ - soil density, dTP₁ and dTP₂ - determined total porosity, PR_{b1} and PR_{b2} - penetration resistance by benchtop analysis, cTP₁ and cTP₂ - calculated total porosity, and DNAt - total soil deoxyribonucleic acid

Figure 2. Simple semivariograms of soil attributes in an Oxisol under no-tillage system, where the alphabetical letters represent the figures of the attributes: (A) PR₁ (MPa); (B) PR₂ (MPa); (C) GM₁ (kg kg⁻¹); (D) GM₂ (kg kg⁻¹); (E) PD₁ (kg dm⁻³); (F) PD₂ (kg dm⁻³); (G) CLA₁ (g kg⁻¹); (H) CLA₂ (g kg⁻¹); (I) SAN₁ (g kg⁻¹); (J) SAN₂ (g kg⁻¹); (K) SIL₁ (g kg⁻¹); (L) SIL₂ (g kg⁻¹); (M) Ma₁ (m³ m⁻³); (N) Ma₂ (m³ m⁻³); (O) Mi₁ (m³ m⁻³); (P) Mi₂ (m³ m⁻³); (Q) SD₁ (kg dm⁻³); (R) SD₂ (kg dm⁻³); (S) dTP₁ (m³ m⁻³); (T) dTP₂ (m³ m⁻³); (U) PR_{b1} (kPa); (V) PR_{b2} (kPa); (W) cTP₁ (m³ m⁻³); (X) cTP₂ (m³ m⁻³) and (Y) DNAt (ng µL⁻¹)



PRi₂ - Penetration resistance, CLA₁ - Clay, SIL₁ - Silt, Ma₁ - Macroporosity, PRb₂ - Penetration resistance by benchtop analysis and DNAt - Total soil deoxyribonucleic acid

Figure 3. Kriging maps of soil attributes in an Oxisol under soybean cultivation in the municipality of Selvíria, MS, where the alphabetical letters represent the figures of the attributes (A) PRi₂ (MPa); (B) CLA₁ (g kg⁻¹); (C) SIL₁ (g kg⁻¹); (D) Ma₁ (m³ m⁻³); (E) PRb₂ (kPa); and (F) DNAt (ng μL⁻¹)

lighter-textured zones to the south and east may demand more frequent irrigation or organic matter enrichment to improve soil moisture retention and nutrient availability.

Similarly, the southwestern portion displayed higher silt content (116 g kg^{-1}) in the 0.00–0.20 m layer, whereas the northern area exhibited lower silt levels. This spatial pattern indicates that the southwestern soils, with their finer texture, tend to retain more water but exhibit slower drainage, which could lead to temporary saturation during rainfall events. For field operations, this implies that mechanized activities should be avoided under high-moisture conditions in these zones to prevent further compaction. In contrast, the northern region may benefit from organic amendments or soil conditioners to enhance water retention. Additionally, Figure 3D shows that the northern area, extending toward the northeast and partially to the southeast, has higher macroporosity (Ma_1) in the first soil layer, with a maximum value of $0.10 \text{ m}^3 \text{ m}^{-3}$. This indicates well-structured soils with adequate aeration and drainage, conditions that are favorable for root development. A substantial portion of the mapped area also displayed intermediate macroporosity values ($0.06 \text{ m}^3 \text{ m}^{-3}$). From a precision agriculture standpoint, these well-structured areas should be maintained with minimal soil disturbance to preserve their favorable physical conditions, whereas zones with lower macroporosity could be targeted for subsoiling or the introduction of cover crops to restore pore continuity and enhance drainage efficiency.

On the other hand, Figure 3E reveals that the northeastern region is characterized by higher penetration resistance in the benchtop analysis (PRb_2), reaching 1.84 MPa in the second soil layer. Penetration resistance is a key physical attribute that directly influences root elongation and is affected by soil preparation systems and machinery traffic. This information allows producers to identify compacted subsurface layers that require remediation through mechanical or biological decompaction. Priority interventions should focus on the northeastern region, where excessive resistance likely constrains root penetration and water infiltration. Implementing site-specific management via precision agriculture tools can optimize energy use and improve soil structural recovery efficiency. Finally, Figure 3F (DNAt map) shows that the southwestern region had the highest concentration of total soil DNA, with $266 \text{ ng } \mu\text{L}^{-1}$, whereas the southeastern and northeastern regions exhibited lower concentrations ($198 \text{ ng } \mu\text{L}^{-1}$). Both the northern and southern portions of the area displayed comparatively low values. This spatial pattern indicates that the southwestern area supports a richer and more active microbial community, potentially enhancing nutrient cycling and crop productivity. Farmers can use this information to preserve biological balance through the application of organic amendments and diversified crop rotations. Conversely, zones with lower DNAt values should receive increased organic inputs and reduced chemical stress to foster microbial diversity and improve soil biological quality. Therefore, integrating these kriging-based spatial maps into precision agriculture systems enables the differentiation of site-specific soil management zones, optimizing input allocation and promoting sustainable yield enhancement. Each mapped attribute provides valuable guidance for identifying areas requiring intervention, preserving soil structural integrity, and supporting resilient crop production systems under no-tillage management.

CONCLUSIONS

1. The greater variability and higher number of linear correlations in the surface layer (0.00–0.20 m) indicate that this is the most sensitive zone to the no-tillage system and soybean root development, establishing it as the primary management layer for crop yield.

2. Total soil DNA correlates significantly with texture and penetration resistance, confirming that physical structure regulates microbial activity in the surface layer and positioning total DNA as a complementary indicator of soil structural quality for soybean.

3. The predominance of the pure nugget effect for most attributes revealed structural homogeneity in the Oxisol under consolidated no-tillage, making broad-scale site-specific management unfeasible for most physical parameters.

4. Variable-rate management is effective only for attributes with confirmed spatial dependence, such as soil texture and penetration resistance. For the remaining attributes, uniform management is recommended, prioritizing traffic control and residue maintenance to ensure long-term soil physical quality.

Contribution of authors: N. E. Mário, R. Montanari contributed to the research design and methodology, data acquisition and analysis, and drafting of the original manuscript. L. S. de Sousa, D. C. Machado, and N. da E. J. Mário contributed to writing the original draft and to the review and editing of the manuscript. J. D. Pedroso, and M. J. Eduardo contributed to the methodology and manuscript writing.

Data Availability Statement: The authors declare that there are no data underlying the text.

Conflict of Interest: None to declare.

Financing statement: This study was financed by National Funds of CAPES – Coordination for the Improvement of Higher Education Personnel, Process no. 88881.979820/2024-01, via the Postgraduate Program in Agronomy - Soil Science, held at the UNESP – São Paulo State University “Júlio de Mesquita Filho”, FCAV – School of Agricultural and Veterinary Sciences, Campus of Jaboticabal, Brazil.

Acknowledgments: This research was supported by CNPq (Conselho Nacional de Desenvolvimento Científico e Tecnológico) and CAPES (Coordenação de Aperfeiçoamento de Pessoal de Nível Superior).

LITERATURE CITED

- Alvares, C. A.; Stape, J. L.; Sentelhas, P. C.; Gonçalves, J. D. M.; Sparovek, G. Köppen's climate classification map for Brazil. *Meteorologische Zeitschrift*, v.22, p.711–728, 2014. <https://doi.org/10.1127/0941-2948/2013/0507>
- Álvarez-Herrera, J. G.; Jaime-Guerrero, M.; Fernández-Pérez, C. J. Spatial variability and geostatistical modeling of soil physical properties under Eucalyptus globulus plantations. *Geomatics*, v.5, e41, 2025. <https://doi.org/10.3390/geomatics5030041>
- Bisolo, A.; Rodrigues, M. F.; Conceição, F. G. D.; Pellegrini, A. Spatial variability and correlation between soil physical properties under no-tillage with and without agricultural terraces. *Brazilian Archives of Biology and Technology*, v.67, e24230802, 2024. <https://doi.org/10.1590/1678-4324-PSSM-2024230802>

- Breure, T. S.; Haefele, S. M.; Hannam, J. A.; Corstanje, R.; Webster, R.; Moreno-Rojas, S.; Milne, A. E. A loss function to evaluate agricultural decision-making under uncertainty: a case study of soil spectroscopy. *Precision Agriculture*, v.23, p.1333-1353, 2022. <https://doi.org/10.1007/s11119-022-09887-2>
- Chakraborty, P.; Singh, N.; Bansal, S.; Sekaran, U.; Sexton, P.; Bly, A.; Anderson, S. H.; Kumar, S. Does the duration of no-till implementation influence depth distribution of soil organic carbon, hydro-physical properties, and computed tomography-derived macropore characteristics? *Soil and Tillage Research*, v.222, 105426, 2022. <https://doi.org/10.1016/j.still.2022.105426>
- CONAB - Companhia Nacional de Abastecimento. Boletim da safra de grãos: 12º levantamento-Safra 2024/25. Brasília: CONAB, 2025. Available on: < https://www.gov.br/conab/pt-br/atuacao/informacoes-agropecuarias/safra/safra-de-graos/boletim-da-safra-de-graos/12o-levantamento-safra-2024-25/e-book_boletim-de-safra-12o-levantamento_2025.pdf >. Accessed in: Sep. 2025.
- Dalchiavon, F. C.; Carvalho, M. P. Correlação linear e espacial dos componentes de produção e produtividade da soja. *Semina: Ciências Agrárias*, v.33, p.541-552, 2012. <https://doi.org/10.5433/1679-0359.2012v33n2p541>
- EMBRAPA - Empresa Brasileira de Pesquisa Agropecuária. Manual de métodos de análise de solo. Rio de Janeiro: Centro Nacional de Pesquisa de Solos. 3.ed, 2018, 575p.
- Filintas, A. Geostatistics precision agriculture modeling on moisture root zone profiles in clay loam and clay soils, using time domain reflectometry multisensors and soil analysis. *Hydrology*, v.12, 183, 2025. <https://doi.org/10.3390/hydrology12070183>
- Freeman, C. L.; Dieudonné, L.; Agbaje, O. B. A.; Žure, M.; Sanz, J. Q.; Collins, M.; Sand, K. K. Survival of environmental DNA in sediments: mineralogic control on DNA taphonomy. *Environmental DNA*, v.5, p.1691-1705, 2023. <https://doi.org/10.1002/edn3.482>
- Jiang, X.; Li, H.; Dai, X.; Li, J.; Liu, Y. An empirical analysis of global soybean supply potential and China's diversified import strategies based on global agro-ecological zones and multi-objective nonlinear programming models. *Agriculture*, v.15, 529, 2025. <https://doi.org/10.3390/agriculture15050529>
- Keshavarzi, A.; De Caires, S. A.; Sintim, H. Y.; Kaya, F.; Kusi, N. Y. O.; Gyasi-Agyei, Y.; Kumar, V. Spatial variability and management zones: Leveraging geostatistics and fuzzy clustering. *Journal of Soil Science and Plant Nutrition*, p.1-19, 2025. <https://doi.org/10.1007/s42729-025-02357-4>
- Laurenti, N.; Pezzopane, J. R.; Guimarães, E. da S.; Bernardi, A. C. de C.; Rodrigues, J. Spatial variability of soil and vegetation properties in integrated production systems. *Revista Brasileira de Engenharia Agrícola e Ambiental*, v.28, e280481, 2024. <https://doi.org/10.1590/1807-1929/agriambi.v28n10e280481>
- Mário, N. E.; Corrêa, A. R.; Montanari, R.; Silva, T. C.; Santos, A. S. dos. Spatial variability of production and bromatological composition of *Brachiaria* and *Panicum* according to the soil chemical attributes in a silvopastoral system with *Eucalyptus*. *Revista de Agricultura Neotropical*, v.11, e8261, 2024. <https://doi.org/10.32404/rean.v11i3.8261>
- Martins, I. M. da S.; Silva, T. C.; Troleis, M. J. B.; Souza, P. T. de; Sena, K. N.; Montanari, R. Linear and spatial variability of eucalyptus dendrometric attributes correlated with the properties of a Typic Haplustox soil (Oxisol) in the Brazilian savannah. *Semina: Ciências Agrárias*, v.43, p.7-24, 2022. <https://doi.org/10.5433/1679-0359.2022v43n1p7>
- Moraes, M. T. de; Olbermann, F. J. R.; Bonetti, J. de A.; Pilegi, L. R.; Costa, M. V. R.; Pacheco, V.; Guimarães, R. M. L. The impacts of cover crop mixes on the penetration resistance model of an Oxisol under no-tillage. *Soil and Tillage Research*, v.242, 106138, 2024. <https://doi.org/10.1016/j.still.2024.106138>
- Neupane, J.; Guo, W.; Cao, G.; Zhang, F.; Slaughter, L.; Deb, S. Spatial patterns of soil microbial communities and implications for precision soil management at the field scale. *Precision Agriculture*, v.23, p.1008-1026, 2022. <https://doi.org/10.1007/s11119-021-09872-1>
- Nidhi; Katiyar, M.; Laik, R. Spatial variability of soil properties using geostatistical approach: a case study in alluvial soils of Samastipur district of Bihar, India. *Arabian Journal of Geosciences*, v.18, 104, 2025. <https://doi.org/10.1007/s12517-025-12250-0>
- Nurbekov, A.; Umarov, S.; Azizov, S.; Umarov, M.; Khaitov, B.; Khalilova, L.; Namozov, F.; Teshaboyev, S. Arid irrigated winter wheat and soybean cropping under conservation tillage systems. *Frontiers in Sustainable Food Systems*, v.9, e1512277, 2025. <https://doi.org/10.3389/fsufs.2025.1512277>
- Plassart, P.; Terrat, S.; Thomson, B.; Griffiths, R.; Dequiedt, S.; Lelievre, M.; Regnier, T.; Nowak, V.; Bailey, M.; Lemanceau, P.; Bispo, A.; Chabbi, A.; Maron, P.-A.; Mougel, C.; Ranjard, L. Evaluation of the ISO standard 11063 DNA extraction procedure for assessing soil microbial abundance and community structure. *PLoS ONE*, v.7, e44279, 2012. <https://doi.org/10.1371/journal.pone.0044279>
- Qiao, C.; Cheng, C.; Ali, T. How climate change and international trade will shape the future global soybean security pattern. *Journal of Cleaner Production*, v.422, e138603, 2023. <https://doi.org/10.1016/j.jclepro.2023.138603>
- Raj, B. V.; Andrade, J. C. de; Cantarella, H.; Quaggio, J. A. Análise química para avaliação da fertilidade de solos tropicais. Campinas: Instituto Agrônomo, 2001. 285p.
- Rodrigues, L. C.; Castro, T. R.; Roque, C. G.; Cunha, F. F. da; Lima Abrantes, F.; Souza, G. V.; Oliveira, J. T. de. Spatial correlation of soybean yield with the chemical attributes of an Oxisol. *Agronomía Colombiana*, v.41, p.1-12, 2023. <https://doi.org/10.15446/agron.colomb.v41n1.107282>
- Silva, A. L.; Mariano, D. de C.; Ebling, Á. A.; Oliveira Neto, C. F. de; Viégas, I. de J. M.; Okumura, R. S. Geostatística para o mapeamento da variabilidade espacial de atributos do solo em sistemas de manejo do solo na Amazônia brasileira. *Revista em Agronegócio e Meio Ambiente*, v.16, e9417, 2023. <https://doi.org/10.17765/2176-9168.2023v16n1e9417>
- Soil Survey Staff. Keys to soil taxonomy. 13.ed. Lincoln: USDA – Natural Resources Conservation Service, 2022. 401p. Available on: <<https://www.nrcs.usda.gov/resources/guides-and-instructions/keys-to-soil-taxonomy>>. Accessed in: Oct. 2025.
- Souza, D. H. S. de; Silva, Ê. F. de F.; Paz-González, A.; Siqueira, G. M.; Dantas, D. da C. Spatial dependence of sugarcane yield according to the altitude and soil physical attributes in a transect. *Revista Caatinga*, v.36, p.897-906, 2023. <http://dx.doi.org/10.1590/1983-21252023v36n417rc>

- Thotakuri, G.; Chakraborty, P.; Singh, J.; Xu, S.; Kovács, P.; Iqbal, J.; Kumar, S. X-ray computed tomography-measured pore characteristics and hydro-physical properties of soil profile as influenced by long-term tillage and rotation systems. *Catena*, v.237, 107801, 2024. <https://doi.org/10.1016/j.catena.2023.107801>
- Torres, J. L. R.; Mazetto Júnior, J. C.; Silveira, B. de S.; Loss, A.; Santos, G. L.; Assis, R. L. de; Lemes, E. M.; Vieira, D. M. da S. Physical attributes of an irrigated Oxisol after Brassicas crops under no-tillage system. *Agronomy*, v.12, e1825, 2022. <https://doi.org/10.3390/agronomy12081825>
- Totti, M. C. V.; Zinn, Y. L.; Silva, S. H. G.; Silva, B. M.; Bocoli, F. A.; Faria, V. L. de; Montes, A. O.; Acuña-Guzman, S. F.; Uezo, A.; Cullen Junior, L.; Fernandes, V. F.; Avanzi, J. C. Organic carbon stocks across various land use systems in sandy Ultisols and Oxisols in Brazil. *Geoderma Regional*, v.40, e00924, 2025. <https://doi.org/10.1016/j.geodrs.2025.e00924>
- Zapata, D.; Rajan, N.; Mowrer, J.; Casey, K.; Schnell, R.; Hons, F. Long-term tillage effect on within-season variations in soil conditions and respiration from dryland winter wheat and soybean cropping systems. *Scientific Reports*, v.11, 2344, 2021. <https://doi.org/10.1038/s41598-021-80979-1>